Signal-Injection-Based Efficient Direct-Determination of Controller Gains and Nonlinear Friction Compensation Values in SPMSM Drives

Chengbo Yang, *Member, IEEE,* Wei Liu, *Senior Member, IEEE,* Bao Song, Xiaotian Xie, *Student Member, IEEE,* Songyan Niu, and K. T. Chau, *Fellow, IEEE*

***Abstract*—This letter proposes an efficient direct-determination method for controller gains and nonlinear friction compensation values of surface-mounted permanent magnet synchronous motor (SPMSM) drive systems, enabling fast deployment and reliable control. Firstly, by leveraging open-loop speed response characteristics of the high-speed region resulting from sequential signal injection, the inertia-to-flux ratio (i.e., the quotient of total inertia to rotor flux linkage) is directly obtained for gain tuning. Secondly, with aiding from an equivalent nonlinear friction model, friction compensation values are directly extracted from the natural-decay speed response data triggered by zero-value signal injection. Departing from conventional approaches, the proposed method circumvents the need for complex model identification and cumbersome procedures, as well as for laborious internal parameter design. Experiments conducted on a 1.2-kW SPMSM drive system confirm the effectiveness of the proposed method.**

***Index Terms*—Control gain tuning, nonlinear friction compensation, signal injection, surface-mounted permanent magnet synchronous motor (SPMSM).**

I. INTRODUCTION

Proportional-integral (PI) controllers, renowned for their structural simplicity and easy implementation, have gained widespread adoption in both current and speed loops of the surface-mounted permanent magnet synchronous motor (SPMSM) drive system [1], [2]. In practice, motors and their drivers are typically designed/supplied as matched pairs so that current-loop PI gains can generally be calibrated prior to shipment from the factory (as seen in products from manufacturers like Yaskawa and Panasonic). Consequently, the tuning of speed-loop PI gains becomes a critical factor in ensuring successful field deployment. Furthermore, speed-loop PI controllers often exhibit limitations in effectively coping with nonlinear friction introduced by transmission components of SPMSM systems, thus necessitating compensation for this nonlinearity [3]-[5]. Although numerous promising approaches for speed-loop tuning and nonlinear friction compensation (NFC) have been reported, several pressing challenges remain, particularly in the following two aspects:

One challenge lies in efficient control gain tuning that combines both high accuracy and low effort. In engineering practice, tuning speed-loop PI gains by trial and error is inadvisable due to potential risks and inefficiency. In fact, the mainstream speed-loop PI controller tuning methods can fall into two categories: model identification (MI)-based indirect methods and objective optimization (O^2)-based direct methods. The former relies on MI techniques (e.g., least squares, extended Kalman filter, and sliding-mode observer) to identify the total inertia and rotor flux linkage of the SPMSM system, thereby indirectly accomplishing gain tuning based on their quotient [6], [7]. The latter constructs the objective function and employs intelligent algorithms (such as genetic algorithm and reinforcement learning) to directly determine optimal PI gains [8]. Compared with O^2-based methods, MI-based ones can effectively avoid the heavy and time-consuming computations caused by high-dimensional searches, repeated iterations, or large-scale data training, thus making it easier to achieve low-effort and accurate controller gain tuning. However, the separate identification of unknown total inertia and rotor flux linkage poses challenges to achieving this goal successfully. On the one hand, the identification methods for these two parameters typically require their own parameter adjustment efforts to ensure convergence and accuracy [9], which inevitably entails a certain time investment. On the other hand, inertia identification relies on the mechanical model, whereas flux linkage estimation is based on the electrical model, thereby complicating the designs and implementations of their identification algorithms. Moreover, during the gain tuning, taking the quotient of these two parameters may amplify identification errors, degrading the tuning quality.

Another challenge is how to determine NFC values in a manner that is both low-effort and precise, thereby enabling an efficient process. Accurate calculation of NFC values hinges on constructing an appropriate nonlinear friction model (NFM). To date, numerous NFMs have been developed (see [4] and references therein), like the Stribeck model, LuGre model, and Dahl model. There are two main approaches dedicated to seeking the accurate establishment of these NFMs. One is the speed-torque testing method, which identifies the NFM by fitting speed and electromagnetic torque data collected from the drive system [10]. While effective, this class of methods requires a large number of experimental tests to guarantee accuracy, making the implementation process time-consuming and tedious. In contrast, a second category of methods, MI-based friction modeling, is capable of obtaining an accurate NFM with fewer experimental tests. This type of method commonly employs heuristic optimization algorithms (e.g., the artificial bee colony algorithm [11]) and observer-based techniques (e.g., parallel observers [12]) to estimate the NFM's parameters. Unfortunately, previously reported NFMs generally involve multiple to-be-estimated parameters, which not only makes the implementation rather complex and challenging, but also demands laborious parameter adjustment for successful identification. After constructing the NFM, calculating NFC values of the SPMSM system also needs to resort to identifying the rotor flux linkage, which further increases the complexity and uncertainty of the compensation.

In this letter, a signal-injection-based method is proposed for the efficient direct-determination of controller gains and NFC values, addressing the above concerns. Overall, this work provides the following main contributions:

1) A novel control gain determination algorithm is proposed. It utilizes speed responses (SRs) in the high-speed region, induced by sequentially injecting ramp and zero-value q-axis current signals in an open speed loop, to directly determine the inertia-to-flux ratio for gain design, thereby greatly reducing tuning effort and ensuring accuracy. Its strengths lie in: *i*) avoiding the cumbersome process and error amplification of separately identifying inertia and rotor flux linkage; *ii*) directly calculating the control gain using SR characteristics, instead of relying on complex O^2-based and MI-based methods; *iii*) requiring no adjustment of its own parameters.

2) An equivalent NFM-based friction compensation algorithm is developed. It directly determines friction compensation values corresponding to each speed by using the NFM's analytical expression and the natural-decay SR triggered by zero-value q-axis current injection, thereby enabling the low-effort and precise compensation. The advantages of this algorithm include: *i*) obviating the need for the separate identification of the conventional NFM's multiple friction parameters and the rotor flux

This work was supported in part by the National Key R&D Project under Grant 2023YFB4704000, in part by the Innovation and Technology Commission under Grant ITP/025/24AP, and in part by The Hong Kong Polytechnic University under Grant P0048560. *(Corresponding author: K. T. Chau.)*

Chengbo Yang, Wei Liu, Xiaotian Xie, and K. T. Chau are with the Research Centre for Electric Vehicles and Department of Electrical and Electronic Engineering, The Hong Kong Polytechnic University, Kowloon, Hong Kong, China (e-mail: chengbo.yang@polyu.edu.hk; wei.liu@polyu.edu.hk; xiaotian.xie@connect.polyu.hk; songyan-nic.niu@polyu.edu.hk; k.t.chau@polyu.edu.hk).

Bao Song is with the National NC System Engineering Research Center and School of Mechanical Science and Engineering, Huazhong University of Science and Technology, Wuhan 430074, China (e-mail: songbao@hust.edu.cn).

linkage; *ii*) requiring only a single experimental test to establish the NFM; *iii*) not needing to design any internal parameters.

II. Mechanical Model Analysis of SPMSM Systems

In industrial applications, the field-oriented control (FOC) with $i_d^* = 0$ is commonly applied to the SPMSM system. Under this control strategy, the mechanical model of a SPMSM system can be formulated as follows [3], [7]:

$$J\dot{\omega}_m = T_e - T_L - T_f = 1.5p_m i_q \psi_r - T_L - T_f \tag{1}$$

where $\omega_m, p_m, i_q, \psi_r, T_e, J, T_L$, and T_f stand for the rotor speed, number of pole pairs, q-axis current, rotor flux linkage, electromagnetic torque, total inertia, load torque, and friction torque, respectively.

It is generally accepted that the friction torque T_f is a function of ω_m. If a linear friction model, i.e., the Coulomb plus viscous friction model, is employed to characterize the friction behavior, then one has

$$T_f = B_r\omega_m + C_r \mathrm{sign}(\omega_m) \tag{2}$$

where B_r and C_r are constants and denote the viscous and Coulomb friction coefficient, respectively. However, in real-world SPMSM drive systems, the friction torque is typically considered as a nonlinear disturbance [3], [4]. When widely used NFMs, such as the Stribeck and LuGre models, are adopted to represent T_f, we have

$$T_f = \begin{cases} \underbrace{B_r\omega_m + C_r\mathrm{sign}(\omega_m) + (f_s - C_r)\mathrm{e}^{-(\omega_m/\omega_s)^2}\mathrm{sign}(\omega_m)}_{\text{Stribeck model}} \\ \underbrace{[\sigma_0 - \dfrac{\sigma_1|\omega_m|}{g(\omega_m)}]z + (\sigma_1 + B_r)\omega_m, \dot{z} = -\dfrac{|\omega_m|z}{g(\omega_m)} + \omega_m}_{\text{LuGre model}} \end{cases} \tag{3}$$

where $g(\omega_m) = [C_r + [f_s - C_r]\mathrm{e}^{-(\omega_m/\omega_s)^2}]/\sigma_0$; f_s and ω_s denote the static friction torque and Stribeck speed, respectively; σ_0, σ_1, and z are the bristle's stiffness coefficient, damping coefficient, and deformation state, respectively.

From (3), it can be observed that at high speeds, the Stribeck model can be represented by (2), since $\mathrm{e}^{-(\omega_m/\omega_s)^2}$ will gradually vanish as the speed increases. Similarly, the LuGre model can also reduce to (2) in the high-speed region, because z approaches $C_r\mathrm{sign}(\omega_m)/\sigma_0$ as time progresses when $g(\omega_m) \approx C_r/\sigma_0$ is satisfied at high speeds (this can be readily seen from the general solution of $\dot{z} = -\sigma_0|\omega_m|z/C_r + \omega_m$). In fact, numerous literature sources, like [4] and [7], have confirmed that when the drive system operates at high speeds, the friction torque can be considered proportional to speed, i.e., the friction behavior in the high-speed region can be accurately characterized by (2). Hence, in the high-speed region, the mechanical model can be rewritten as

$$J\dot{\omega}_m = 1.5p_m i_q \psi_r - T_L - B_r\omega_m - C_r\mathrm{sign}(\omega_m). \tag{4}$$

III. Proposed Method

A. Efficient Direct-Determination of PI Gains Using Signal Injection

In practical applications, the speed-loop PI controller can be designed/tuned based on the following equation [5], [6]:

$$k_{sp} = \frac{J\omega_{sc}}{1.5p_m\psi_r} = (\frac{J}{\psi_r})\frac{\omega_{sc}}{1.5p_m}, k_{si} = \frac{J\omega_{sc}^2}{7.5p_m\psi_r} = (\frac{J}{\psi_r})\frac{\omega_{sc}^2}{7.5p_m} \tag{5}$$

where k_{sp} and k_{si} denote the proportional and integral gains of the speed-loop PI controller, respectively; ω_{sc} is the desired bandwidth.

From (5), it is evident that once J/ψ_r (i.e., inertia-to-flux ratio) is known, the PI gains can be determined. In this letter, with the speed loop open, a ramp current is injected into the q-axis, and the resulting SR in the high-speed region is utilized to directly calculate ψ_r/B_r. Then, B_r/J is directly determined by analyzing the high-speed region's natural-decay SR triggered by the zero-value q-axis current injection. Finally, J/ψ_r is obtained using ψ_r/B_r and B_r/J.

Define i_q^{in} as the q-axis injection current. When the ramp current signal injected into the q-axis is designed as $i_q^{in} = \lambda t$ (where λ is the slope and satisfies $\lambda > 0$), T_e can be calculated as $T_e = 1.5p_m\psi_r\lambda t$.

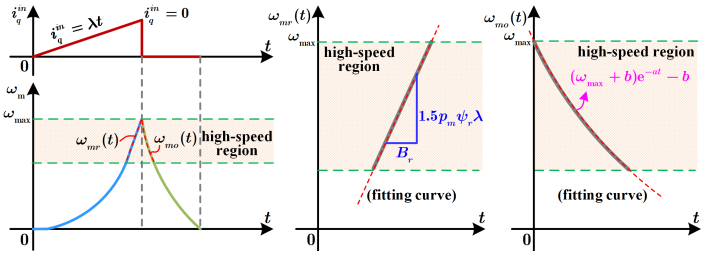

Fig. 1. Principle of calculating ψ_r/B_r and B_r/J.

Therefore, under such an injection condition, the mechanical model in the high-speed region can be derived from (4) as $J\dot{\omega}_{mr} = 1.5p_m\psi_r\lambda t - T_L - B_r\omega_{mr} - C_r$, where ω_{mr} denotes the high-speed region's SR due to injecting the ramp current signal. Considering the no-load condition before the drive system is put into work operation, the above equation can be rewritten as

$$J\dot{\omega}_{mr} = 1.5p_m\psi_r\lambda t - B_r\omega_{mr} - C_r. \tag{6}$$

Then, through analytically solving (6), we can derive the formula describing the high-speed region's SR induced by the ramp current injection, as follows:

$$\omega_{mr}(t) = C_1\mathrm{e}^{-(B_r/J)t} + \frac{1.5p_m\psi_r\lambda}{B_r}t - \frac{B_rC_r + 1.5p_m\psi_r\lambda J}{B_r^2} \tag{7}$$

where C_1 is a constant. It is noteworthy that as time increases, the term $C_1\mathrm{e}^{-(B_r/J)t}$ in (7) will gradually approach zero. Once this term vanishes, (7) will become a straight line with a slope of $1.5p_m\psi_r\lambda/B_r$. Obviously, this slope contains the value of ψ_r/B_r. By fitting this straight line, its slope can be determined, thereby enabling the calculation of ψ_r/B_r. Given that the injected q-axis current increases in a ramp manner, the motor speed will gradually rise until it reaches the allowable maximum value $\omega_{\max}$. It is well known that, under $i_d^* = 0$ control, a faster-varying q-axis current will lead to a more rapid increase in motor speed. Thus, the time required to accelerate from standstill to $\omega_{\max}$ is negatively correlated with λ. This implies that, to promote the elimination of the term $C_1\mathrm{e}^{-(B_r/J)t}$, λ needs to be assigned a small value. Later, a simple procedure will be designed to determine an appropriate λ for any SPMSM system. Assuming the slope of the fitted straight line is $r_{\psi-B}$, ψ_r/B_r can be calculated as

$$\psi_r/B_r = r_{\psi-B}/(1.5p_m\lambda). \tag{8}$$

When the drive system is accelerated to $\omega_{\max}$ by injecting the ramp current signal, the motor speed will naturally decay to zero if the injected q-axis current is suddenly changed to $i_q^{in} = 0$. During this decay-decay process, T_e is zero, so the mechanical model in the high-speed region becomes $J\dot{\omega}_{mo} = -B_r\omega_{mo} - C_r$, where ω_{mo} refers to the SR of the high-speed region during the zero-value current injection. By analytically solving this equation, the expression for the high-speed region's natural-decay SR induced by the injection of $i_q^{in} = 0$ can be derived, i.e., $\omega_{mo}(t) = C_2\mathrm{e}^{-(B_r/J)t} - C_r/B_r$ (where C_2 is a constant). Assuming the moment when the speed begins to decay is regarded as the initial time point, one has $\omega_{mo}(0) = \omega_{\max}$. As a result, $C_2 = \omega_{\max} + C_r/B_r$. Then, we can obtain

$$\omega_{mo}(t) = (\omega_{\max} + C_r/B_r)\mathrm{e}^{-(B_r/J)t} - C_r/B_r. \tag{9}$$

Thus, by fitting the high-speed region's natural-decay SR $\omega_{mo}(t)$ to the model $\omega_{mo}(t) = (\omega_{\max} + b)\mathrm{e}^{-at} - b$ (where a and b are constants), the value of B_r/J can be determined. Assuming the fitted value of B_r/J is r_{B-J}, the inertia-to-flux ratio can then be calculated as

$$J/\psi_r = 1/[(\psi_r/B_r)\cdot(B_r/J)] = 1.5p_m\lambda/(r_{\psi-B}r_{B-J}). \tag{10}$$

With (10), PI gains in (5) can be directly calculated. Fig.1 shows the principle of obtaining ψ_r/B_r and B_r/J in detail.

B. Speed-Decay-Based Efficient Direct-Determination of NFC Values

As previously mentioned, the friction torque is a function of speed, i.e., it can be expressed as the product of speed and an unknown component. For instance, the Stribeck model can be formulated as the

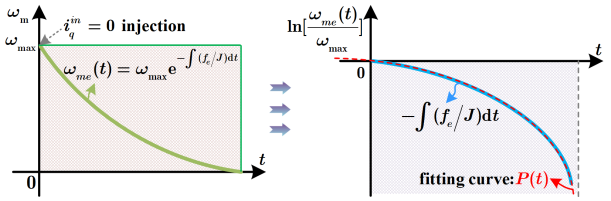

Fig. 2. Principle of calculating $\int -(f_e/J)\mathrm{d}t$.

product of ω_m and $B_r+[C_r\mathrm{sign}(\omega_m)+(f_s-C_r)\mathrm{e}^{-(\omega_m/\omega_s)^2}\mathrm{sign}(\omega_m)]/\omega_m$. Inspired by this, this letter proposes an equivalent NFM to simplify the calculation process of friction compensation values, as follows:

$$T_f = f_e\omega_m \tag{11}$$

where f_e stands for the equivalent friction coefficient, which varies dynamically with the rotor speed ω_m.

Generally, in the FOC with $i_d^{in}=0$, the friction compensation value i_{com} can be calculated by $i_{com}=T_f/(1.5p_m\psi_r)$ [3]. If the friction torque is given by (11), then we have $i_{com}=f_e\omega_m/(1.5p_m\psi_r)$. It is evident that once f_e/ψ_r is determined, i_{com} can be obtained. In this letter, the friction compensation value corresponding to each speed is directly calculated based on (11) and by utilizing the natural-decay SR induced by injecting the zero-value q-axis current.

In the process of calculating B_r/J, the zero-value q-axis current injection enables the complete collection of natural-decay SR data within the speed range of zero to $\omega_{\max}$. Since T_e is absent after the natural decay occurs, it follows from (1) and (11) that during this period, the mechanical model under the no-load condition can be expressed as $J\dot{\omega}_{me}=-f_e\omega_{me}$, where ω_{me} denotes the natural-decay SR triggered by the injection of $i_q^{in}=0$. Then, through analytically solving this equation, the formula describing the relationship between the natural-decay SR and time can be derived as

$$\omega_{me}(t)=\omega_{\max}\mathrm{e}^{-\int(f_e/J)\mathrm{d}t}. \tag{12}$$

Applying the natural logarithm to both sides of (12) yields

$$\ln[\omega_{me}(t)]-\ln(\omega_{\max})=\ln[\omega_{me}(t)/\omega_{\max}]=\int -(f_e/J)\mathrm{d}t. \tag{13}$$

If f_e/J can be obtained, then f_e/ψ_r can be directly calculated by multiplying f_e/J by J/ψ_r. To this end, this letter uses a polynomial $P(t)$ to fit (13), i.e.,

$$\int -(f_e/J)\mathrm{d}t = P(t)=p_ht^h+p_{h-1}t^{h-1}+\cdots+p_1t+p_0 \tag{14}$$

where $p_x(x=0,1,2,\cdots,h-1,h)$ is the fitting coefficient; h is the order of $P(t)$. Fig. 2 illustrates the principle of calculating $\int -(f_e/J)\mathrm{d}t$. Based on (14), we have $f_e/J=-\dot{P}(t)=-(hp_ht^{h-1}+(h-1)p_{h-1}t^{h-2}+\cdots+p_2t+p_1)$. Thus, one can obtain

$$f_e/\psi_r=(f_e/J)\cdot(J/\psi_r)=-1.5\dot{P}(t)\,p_m\lambda/(r_{\psi-B}r_{B-J}) \tag{15}$$

which characterizes the relationship between f_e/ψ_r and the time. Since during the natural-decay process, there exists a one-to-one correspondence between the time and the rotor speed within the speed range of zero to $\omega_{\max}$, the mapping curve between f_e/ψ_r and ω_m can be obtained easily, thereby establishing a lookup table describing the corresponding relationship between f_e/ψ_r and ω_m. Let $G(\cdot)$ denotes this mapping relationship (e.g., $G(\varpi)$ represents the value of f_e/ψ_r corresponding to the speed ϖ in the lookup table), then we can directly calculate the NFC value as $i_{com}=G(\omega_m)\omega_m/(1.5p_m)$.

C. Implementation of the Proposed Method

The determination of PI gains and NFC values is closely related to the calculations of ψ_r/B_r, B_r/J, and f_e/J. This letter develops a simple automatic procedure for implementing the calculations of ψ_r/B_r, B_r/J, and f_e/J, whose working principle is shown in Fig. 3. The working principle is further elucidated below:

As shown in Fig. 3(a), the calculation of ψ_r/B_r is performed first. Calculating ψ_r/B_r needs the slope $r_{\psi-B}$ of the straight-line equation obtained by linear fitting. As analyzed in Section III-A, λ should be

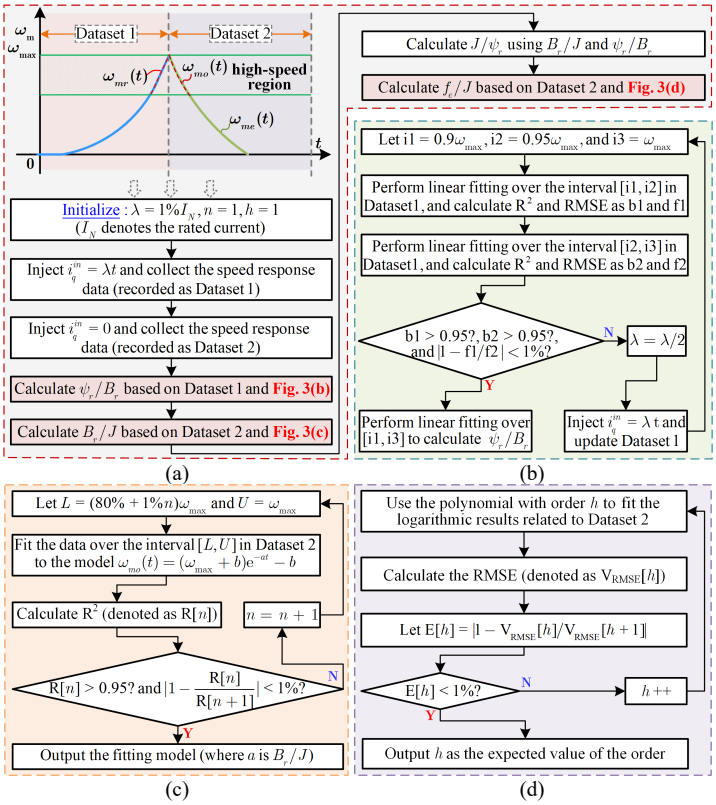

Fig. 3. Implementation procedure of calculating ψ_r/B_r, B_r/J, and f_e/J. (a) Overall implementation flowchart. (b) Flowchart of calculating ψ_r/B_r. (c) Flowchart of calculating B_r/J. (d) Automatic selection of fitting order.

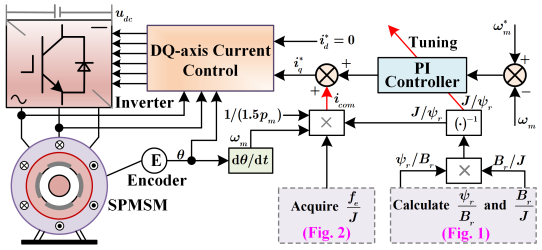

Fig. 4. Overall block diagram of the proposed method.

selected to be sufficiently small. Essentially, a small λ is intended to ensure that the SR data fitting interval used for calculating ψ_r/B_r is located in the high-speed region where the term $C_1\mathrm{e}^{-(B_r/J)t}$ in (7) has already converged to near zero, achieving high accuracy. To autonomously determine an appropriate λ for any SPMSM system, this letter uses the coefficient of determination (denoted as R^2) and the root mean square error (RMSE) as evaluation metrics. As shown in Fig. 3(b), when the R^2 values in the two selected equal-length intervals both reach high levels and their RMSE values are almost consistent, it can be considered that the SR data in these two intervals are on the same straight-line equation (i.e., the term $C_1\mathrm{e}^{-(B_r/J)t}$ is already negligible). At this point, the value of λ can be deemed suitable. Then, the combined interval formed by these two regions can be chosen for linear fitting to accurately calculate ψ_r/B_r.

Subsequently, the calculation of B_r/J is conducted. Notably, the calculation of B_r/J requires establishing the model $\omega_{mo}(t)=(\omega_{\max}+b)\mathrm{e}^{-at}-b$ through curve fitting. Meanwhile, it is necessary to ensure that the fitted data interval is positioned within the high-speed region of the natural-decay SR. Similarly, to determine an appropriate fitting interval, the R^2 metric is introduced as the evaluation criterion. As shown in Fig. 3(c), if the R^2 value in the current fitting interval has reached a high level and its change relative to the previous fitting interval is extremely small (i.e., R^2 tends to stabilize), then it can be considered that the current interval conforms well to the fitting model's target expression, thereby obtaining the accurate B_r/J.

After obtaining the values of ψ_r/B_r and B_r/J, calculating f_e/J

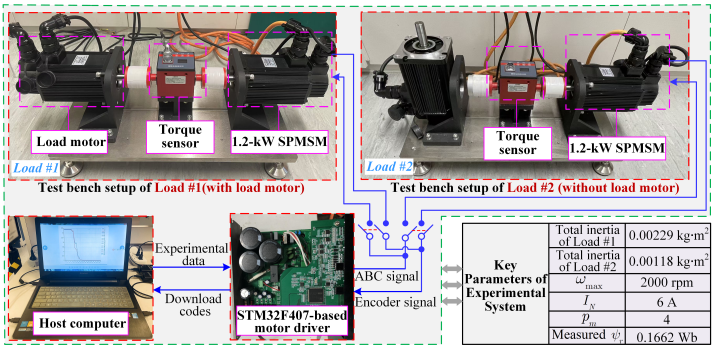

Fig. 5. Experimental system.

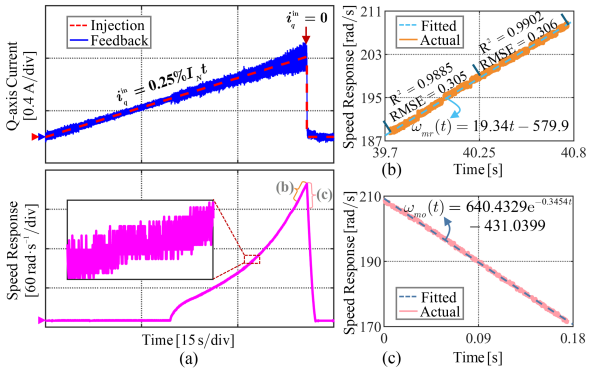

Fig. 6. Calculation of J/ψ_r under Load #1. (a) SR curves induced by injecting $i_q^{in}=\lambda t$ and $i_q^{in}=0$. (b) Determination of $r_{\psi-B}$. (c) Determination of r_{B-J}.

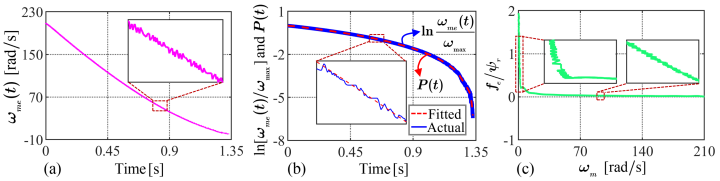

Fig. 7. Calculation of f_e/ψ_r under Load #1. (a) Natural-decay SR over $[0,\omega_{\max}]$. (b) Calculation and fitting of $\ln[\omega_{me}(t)/\omega_{\max}]$. (c) Mapping relationship between f_e/ψ_r and ω_m.

only requires determining $P(t)$. Due to the presence of noise data in practical polynomial fitting, the fitting error gradually stabilizes as the order increases. Therefore, Fig. 3(d) designs an automatic order selection algorithm. It uses the relative change rate of RMSE from the fitting results as the criterion for selecting the suitable value of order h, thereby automatically acquiring the expression of $P(t)$.

Fig. 4 shows the overall block diagram of the proposed method.

IV. Experimental Verification

To verify the effectiveness of the proposed method, experimental investigations are conducted based on the test system shown in Fig. 5. As depicted in Fig. 5, two load conditions with different inertias are configured for the 1.2-kW drive motor:

- Load #1 (with load motor): A load motor, a torque sensor, and two couplings are connected to the drive motor, yielding a total system inertia of 0.00229 kg·m².
- Load #2 (without load motor): The load motor is disconnected from the setup for Load #1, resulting in a total system inertia of 0.00118 kg·m².

1) Determination of J/ψ_r and f_e/ψ_r: Fig. 6 presents the test results for Load #1, obtained during the execution of the implementation procedure shown in Fig. 3. Fig. 6(a) provides the SR curves when $i_q^{in}=\lambda t$ and $i_q^{in}=0$ are sequentially injected. From Fig. 6(b), it can be observed that when λ is assigned a value of $0.25\%I_N$ by executing Fig. 3(b), the R^2 and RMSE values in the intervals $[0.9\omega_{\max},0.95\omega_{\max}]$ and $[0.95\omega_{\max},\omega_{\max}]$ can satisfy the specified judgment criteria. Thus, under Load #1, a suitable value for λ is $0.25\%I_N$. This enables "$(1.5p_m\psi_r\lambda/B_r)t-(B_rC_r+1.5p_m\psi_r\lambda J)/B_r^2$" to be accurately fitted as "$19.34t-579.9$", i.e., $r_{\psi-B}=19.34$. Additionally, as shown in Fig. 6(c), a suitable interval determined by

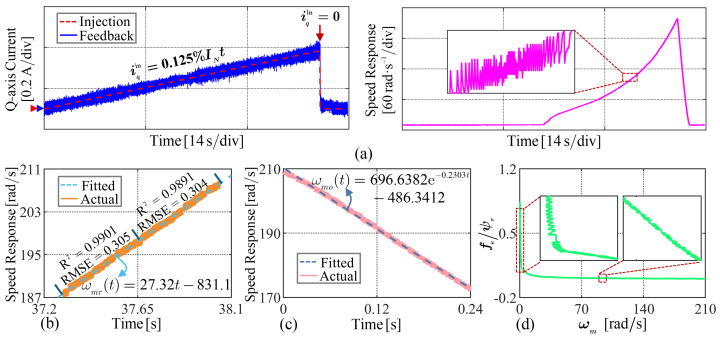

Fig. 8. Calculation of J/ψ_r and f_e/ψ_r under Load #2. (a) SR curves induced by injecting $i_q^{in}=\lambda t$ and $i_q^{in}=0$. (b) Determination of $r_{\psi-B}$. (c) Determination of r_{B-J}. (d) Mapping relationship between f_e/ψ_r and ω_m.

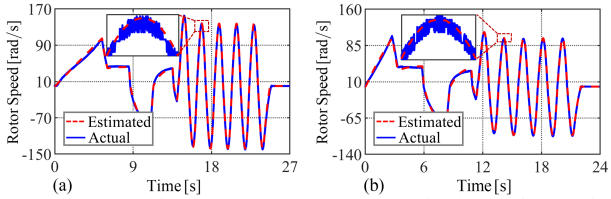

Fig. 9. Accuracy verification test. (a) Accuracy evaluation under Load #1. (b) Accuracy evaluation under Load #2.

executing Fig. 3(c) is $[82\%\omega_{\max},\omega_{\max}]$. Within this interval, the fitted result of $\omega_{mo}(t)$ is $640.4329e^{-0.3454t}-431.0399$, i.e., $r_{B-J}=0.3454$. Therefore, according to (10), J/ψ_r can be calculated as 0.01347, which closely matches the true value shown in Fig. 5.

Subsequently, the NFC value under Load #1 is calculated. Fig. 7(a) depicts the natural-decay SR of Load #1 over the interval $[0,\omega_{\max}]$. And the curve of $\ln[\omega_{me}(t)/\omega_{\max}]$ is provided in Fig. 7(b). By fitting this curve, we can obtain the expression of $P(t)$, as indicated by the red dashed curve in Fig. 7(b). Based on this fitted result, the mapping curve between f_e/ψ_r and ω_m, shown in Fig. 7(c), can be derived, thereby enabling the establishment of the corresponding lookup table.

Furthermore, to fully evaluate the proposed method, related tests are performed under Load #2. The corresponding experimental results are shown in Fig. 8. It can be readily seen that when the value of λ is autonomously determined to be $0.125\%I_N$ by executing the procedure in Fig. 3(b), the specified judgment criteria are satisfied. This implies that, unlike under Load #1, the appropriate value of λ under Load #2 is $0.125\%I_N$. Figs. 8(b) and 8(c) indicate that the calculated $r_{\psi-B}$ and r_{B-J} under Load #2 are 27.32 and 0.2303, respectively. Thus, we have $J/\psi_r=0.00715$, which is very close to the true value given in Fig. 5. In addition, the mapping relationship between f_e/ψ_r and ω_m under Load #2 is shown in Fig. 8(d).

2) Accuracy Assessment: To evaluate the calculation accuracy of J/ψ_r and f_e/ψ_r, the following verification process is conducted: *i*) Inject a random *q*-axis current command under open-loop speed control, and collect the actual *q*-axis current and rotor speed; *ii*) The collected *q*-axis current, together with the calculated J/ψ_r and f_e/ψ_r, are substituted into the mechanical model $\dot{\omega}_m=1.5p_m i_q/(J/\psi_r)-(f_e/\psi_r)[1/(J/\psi_r)]\omega_m$ to calculate the estimated speed, which is then compared with the actual speed to assess the accuracy. The evaluation results for Load #1 and Load #2 are shown in Fig. 9. Both Figs. 9(a) and 9(b) indicate that the estimated speed aligns closely with the actual one, demonstrating a high calculation accuracy of J/ψ_r and f_e/ψ_r under Load #1 and Load #2.

3) Comparison With Previous Methods: As stated in Section I, the high efficiency of our method in determining the control gains and NFC values is manifested in two aspects: low overall effort and good accuracy. Undoubtedly, our method outperforms existing approaches in terms of tuning/compensation effort. This is mainly attributed to the fact that our method avoids complex MI algorithms, laborious internal parameter design, and cumbersome procedures. Thus, to further demonstrate its superiority, a comparative accuracy

TABLE I
COMPARATIVE METHODS

Methods		Implementation effort			Factors affecting Tuning/Compensation Accuracy	
		Design and procedural complexity	*Internal parameter tuning*	*HW reqs.*	*Internal parameter configs.*	*Error ampl.*
Comp. methods	***Method I***: [12] + [13]	High	High	Low	Affected	Affected
	Method II: [5] + [13]	High	High	Low	Affected	Affected
	Method III: [11] + [13]	High	High	High	Affected	Affected
Proposed method		Low	None	Low	Unaffected	Unaffected

NOTE: "Comp." = "Comparison"; "HW reqs." = "Hardware requirements"; "configs." = "configurations"; "ampl." = "amplification".

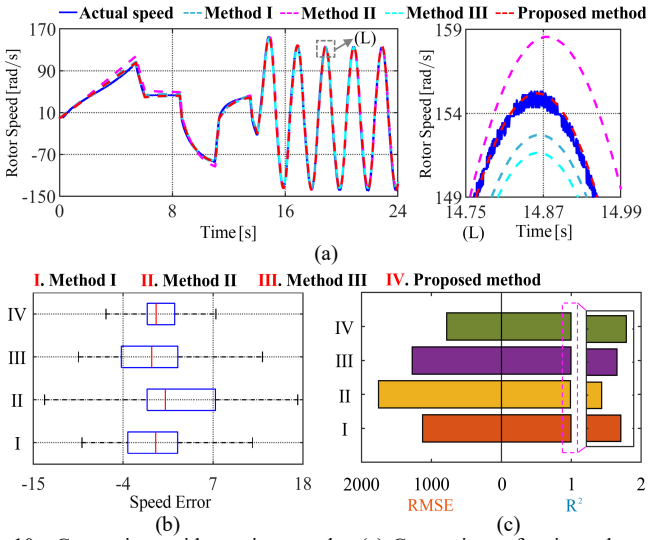

Fig. 10. Comparison with previous works. (a) Comparison of estimated speeds. (b) Boxplot comparison of errors. (b) Comparison of RMSE and R^2 metrics.

assessment is necessary. However, since existing methods rarely consider control gain tuning and NFC simultaneously, it is difficult to directly select a fair single benchmark for comparison. Of note, Section I has already pointed out that the MI-based technical route is more competitive for achieving controller gain tuning and NFC. Accordingly, as shown in Table I, this letter selects several advanced methods for the simultaneous identification of inertia and nonlinear friction-related parameters (i.e., [5], [11], and [12]) and combines them with the rotor flux linkage estimation method [13] to form three competitive comparison methods, thereby ensuring a fair comparison.

To intuitively present the comparison results, this letter follows the above accuracy verification process, i.e., the identification results from each comparative method are substituted into its identification model to calculate the estimated speed, which is then compared with the actual speed. Here, this letter takes Load #1 as an example to conduct the related comparison tests, and the corresponding results are shown in Fig. 10. We can see from Fig. 10(a) that, compared to our method, the estimated speeds from the comparative methods deviate more significantly from the actual speed. Moreover, as shown in Fig. 10(b) and 10(c), the comparison methods perform worse than our method in terms of boxplot statistics, R^2 metric, and RMSE metric. These experimental results indicate that our method can yield more accurate control gains and NFC values. This superiority stems from two key aspects: *i*) our method directly calculates J/ψ_r and f_e/ψ_r, avoiding the error amplification that results from division operations; *ii*) these comparative methods are affected by internal parameter selections, whereas our method does not involve any to-be-adjusted parameters.

4) Control Effect Test: Here, taking Load #1 as an example, the control effect regarding the proposed method is evaluated. Fig. 11 presents the control effect with PI gain tuning and NFC implemented

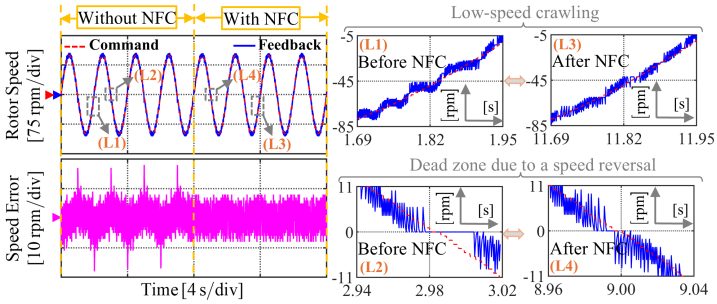

Fig. 11. Control performance evaluation of the PMSM system using our method.

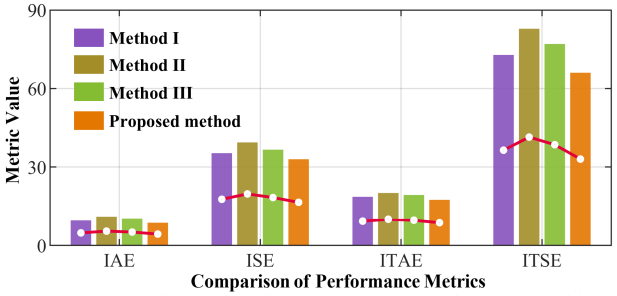

Fig. 12. Comparison of control performance metrics for the SPMSM drive system applying different methods.

using the calculated J/ψ_r and f_e/ψ_r (note that $\omega_{sc} = 20$ rad/s). We can see that the designed PI controller achieves stable and accurate speed tracking under the given sinusoidal speed reference, with nearly zero overshoot and phase delay. Furthermore, by comparing the results before and after NFC, it can be observed that activating NFC significantly improves speed tracking accuracy (the maximum tracking error is reduced by approximately 55.6%). In addition, it is noticed from Fig. 11 that compensating for nonlinear friction can markedly alleviate low-speed crawling and the dead zone arising from speed reversal. The above test outcomes further verify the effectiveness of the proposed method.

Furthermore, to highlight the importance of the proposed method's higher accuracy for optimizing control performance, a comprehensive control performance comparison for the SPMSM system applying different methods listed in Table I is conducted. In this comparison, four typical control performance metrics, including the integral absolute error (IAE), integral square error (ISE), integral time absolute error (ITAE), and integral time square error (ITSE), are evaluated. The comparative evaluation results are summarized in Fig. 12. From there, we can observe that when the proposed method is applied for the PI gain tuning and NFC of the SPMSM system, all of these metrics exhibit significant improvement. For instance, the ITSE metric value achieved by our method is reduced by more than 20% relative to Method II. These test results strongly indicate that the higher accuracy of the proposed method can be directly translated into superior control performance, thereby underscoring its pronounced advantages for practical applications.

V. CONCLUSION

In this letter, an efficient direct-determination method for control gains and NFC values of the SPMSM drive system is proposed. By utilizing SRs that arise from sequentially injecting ramp and zero-value currents into the *q*-axis under the open speed loop condition, the proposed method determines J/ψ_r and f_e/ψ_r in a manner that is both low-effort and accurate, enabling efficient speed-loop PI tuning and friction compensation. In contrast to existing methods, our method directly calculates control gains and NFC values from open-loop SR characteristics, rather than relying on complex MI-based approaches and cumbersome procedures. Moreover, this method precludes the need for laborious internal parameter design. Experimental tests on a 1.2-kW SPMSM system have validated the feasibility of the proposed method. Furthermore, the SPMSM system using our method has been

proven to attain stable and accurate speed tracking. Future work will explore controller tuning and friction compensation for scenarios where J and ψ_r may vary during system operation.

REFERENCES

[1] P. Chen, Y. Luo, H. Gan, Y. Liu, and Y. Chen, "A current- and speed-loop decoupling controller for SPMSM under periodic disturbances," *IEEE Trans. Power Electron.*, vol. 39, no. 6, pp. 6889–6902, Jun. 2024.

[2] Y. Fan, J. Chen, Q. Zhang, and M. Cheng, "An improved inertia disturbance suppression method for PMSM based on disturbance observer and two-degree-of-freedom PI controller," *IEEE Trans. Power Electron.*, vol. 38, no. 3, pp. 3590–3599, Mar. 2023.

[3] C. Yang, B. Song, Y. Xie, S. Zheng, and X. Tang, "Adaptive identification of nonlinear friction and load torque for PMSM drives via a parallel-observer-based network with model compensation," *IEEE Trans. Power Electron.*, vol. 38, no. 5, pp. 5875–5897, May 2023.

[4] C. Wang, J. Peng, and J. Pan, "A novel friction compensation method based on Stribeck model with fuzzy filter for PMSM servo systems," *IEEE Trans. Ind. Electron.*, vol. 70, no. 12, pp. 12124–12133, Dec. 2023.

[5] W.-S. Huang, C.-W. Liu, P.-L. Hsu, and S.-S. Yeh, "Precision control and compensation of servomotors and machine tools via the disturbance observer," *IEEE Trans. Ind. Electron.*, vol. 57, no. 1, pp. 420–429, Jan. 2010.

[6] S.-K. Sul, *Control of Electric Machine Drive Systems*. Hoboken, NJ, USA: Wiley, 2010, pp. 198–201.

[7] S. Kim, "Moment of inertia and friction torque coefficient identification in a servo drive system," *IEEE Trans. Ind. Electron.*, vol. 66, no. 1, pp. 60–70, Jan. 2019.

[8] M. Nicola and C.-I. Nicola, "Tuning of PI speed controller for PMSM control system using computational intelligence," in *Proc. Int. Symp. Power Electron.*, Novi Sad, Serbia, 2021, pp. 1–6.

[9] C. Yang, B. Song, Y. Xie, S. Lu, and X. Tang, "Stable simultaneous inertia and disturbance torque identification for SPMSM drive systems subject to mismatched rotor flux linkage," *IEEE J. Emerg. Sel. Topics Power Electron.*, vol. 10, no. 2, pp. 2445–2462, Apr. 2022.

[10] W. Lin *et al.*, "Adaptive extended state observer-based velocity-free servo tracking control with friction compensation," *IEEE Trans. Syst. Man. Cybern.: Syst.*, vol. 54, no. 1, pp. 2–11, Jan. 2024.

[11] R. Szczepanski, T. Tarczewski, L. J. Niewiara, and D. Stojic, "Identification of mechanical parameters in servo-drive system," in *Proc. IEEE 19th Int. Power Electron. Motion Control Conf.*, 2021, pp. 566–573.

[12] D. Xiang, J. Yang, Y. Hao, and G. Xu, "Parallel-cascaded parameter identification scheme for PMSM-driven servo systems during self-commission," *IEEE Trans. Ind. Electron.*, vol. 72, no. 2, pp. 1914–1924, Feb. 2025.

[13] C. Yang, B. Song, J. Jatskevich, H. Zhang, and C. H. T. Lee, "Normal-operation-undisturbed magnet flux linkage monitoring in PMSM drives via a mechanical-model-based dual time-scale approach," *IEEE Trans. Ind. Inform.*, vol. 20, no. 4, pp. 6266–6279, Apr. 2024.